

Article

# Prediction of a Material Property Gradient near the Friction Surface in Axisymmetric Extrusion and Drawing

Elena Lyamina <sup>1,2</sup><sup>1</sup> Metal Forming Department, Samara National Research University, 334086 Samara, Russia; lyamina@inbox.ru<sup>2</sup> Laboratory for Technological Processes, Ishlinsky Institute for Problems in Mechanics RAS, 119526 Moscow, Russia

**Abstract:** The present paper provides a theoretical prediction of the evolution of material properties near the friction surface in axisymmetric extrusion and drawing. The method employed is based on the strain rate intensity factor and uses empirical equations that connect the integrated strain rate intensity factor with the thickness of a narrow layer of intensive plastic deformation and the hardness of the surface layer. The material obeys Hosford's yield criterion. Therefore, the empirical equations above are reformulated in terms of the work rate intensity factor. Since no numerical method is available, the strain rate and work rate intensity factors are determined from an approximate solution. The solution reveals the effect of process and material parameters on the thickness of a layer of intensive plastic deformation and the hardness of the surface layer. Since the solution is semi-analytical, it is straightforward to use its results to design the metal forming processes.

**Keywords:** extrusion; drawing; friction; gradient of material properties; strain rate intensity factor; work rate intensity factor



**Citation:** Lyamina, E. Prediction of a Material Property Gradient near the Friction Surface in Axisymmetric Extrusion and Drawing. *Metals* **2022**, *12*, 1310. <https://doi.org/10.3390/met12081310>

Academic Editors: Marcello Cabibbo and Miguel Cervera

Received: 6 July 2022

Accepted: 2 August 2022

Published: 4 August 2022

**Publisher's Note:** MDPI stays neutral with regard to jurisdictional claims in published maps and institutional affiliations.



**Copyright:** © 2022 by the author. Licensee MDPI, Basel, Switzerland. This article is an open access article distributed under the terms and conditions of the Creative Commons Attribution (CC BY) license (<https://creativecommons.org/licenses/by/4.0/>).

## 1. Introduction

Friction is unavoidable in most metal forming processes. It significantly contributes to redundant work and the non-uniformity of deformation. Because it is impossible to avoid friction and it is very difficult to propose an accurate friction law, it is desirable to develop a method that allows for the prediction of material properties near frictional surfaces. The present paper concerns such a method that requires no realistic friction law.

Metal forming processes often generate high gradients of material properties within a narrow layer near frictional interfaces [1]. These layers are advantageous for some applications [2,3]. Theoretical predictions on the effect of process parameters on the gradient of material properties are required for designing the processes. The present paper considers the process of axisymmetric direct extrusion. Its results also apply to the process of drawing.

A vast amount of literature is devoted to experimental studies of the generation of material properties near the friction surface in extrusion and drawing [4–12]. These studies have shown that the evolution of material properties near frictional interfaces is affected by many process conditions. Therefore, it is reasonable to expect that the process conditions can be chosen such that the process generates a desirable distribution of material properties. To this end, a theoretical method that allows for the parameter characterizing material properties to be calculated is required. Conventional methods are unsuitable because the evolution of material properties near frictional interfaces does not obey the constitutive equations that are valid in bulk. The present paper employs the method proposed in [13]. This method is based on the strain rate intensity factor introduced in [14].

The strain rate intensity factor should be determined from the solution of a singular boundary value problem in plasticity theory. The standard finite element method cannot solve such problems [15]. The only available numerical method is based on the characteristics theory and applies to plane strain problems [16]. Therefore, this method cannot also

be used to analyze axisymmetric extrusion and drawing. It has been shown in [17] that an efficient approximate method of analyzing these processes can be based on solutions for the material flow through infinite converging channels. The present paper employs this method. It is assumed that the material obeys Hosford's yield criterion [18]. The solutions for the material flow through infinite converging channels for this yield criterion are available [19,20]. However, these solutions do not provide the strain rate intensity factor necessary for applying the method [13].

The present paper extends the solution [20] to calculate the strain rate intensity factor. Paper [13] provides empirical equations that connect the integrated strain rate intensity factor with the thickness of the layer of intensive plastic deformation and the hardness of the surface layer. These equations are valid for aluminum 6061. They are based on experiments under plane strain conditions. In this case, all isotropic pressure-independent yield criteria have the same form. The present paper proposes to replace the strain rate intensity factor with the work rate intensity factor to apply the experimental results [13] to an arbitrary yield criterion in the case of three-dimensional deformation. This approach has also been used in [21] to extend the concept of the strain rate intensity factor in plane strain deformation of isotropic materials to anisotropic materials.

## 2. Statement of the Problem

A rod of initial radius  $R_0$  is extruded through a conical die (total angle  $2\theta_0$ ). The final radius of the rod is  $r_0$  (Figure 1). It is convenient to use a spherical coordinate system  $(\rho, \theta, \varphi)$ . The axis of symmetry of the process corresponds to  $\theta = 0$ . The equation of the die surface is  $\theta = \theta_0$ . The solution is independent of  $\varphi$ .

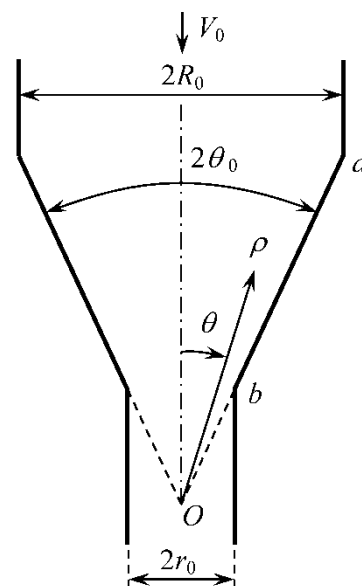


**Figure 1.** Schematic diagram of the extrusion process.

The stress components in the spherical coordinate system are denoted as  $\sigma_{\rho\rho}$ ,  $\sigma_{\theta\theta}$ ,  $\sigma_{\varphi\varphi}$ ,  $\sigma_{\rho\theta}$ ,  $\sigma_{\rho\varphi}$ , and  $\sigma_{\varphi\theta}$ . The components  $\sigma_{\rho\varphi}$  and  $\sigma_{\varphi\theta}$  vanish. Therefore,  $\sigma_{\rho\rho}$  is one of the principal stresses. The other principal stresses are denoted as  $\sigma_1$  and  $\sigma_3$ . With no loss of generality, it is assumed that  $\sigma_1 > \sigma_3$ .

The material obeys Hosford's yield criterion [18]. In the case under consideration, this yield criterion reads

$$(\sigma_1 - \sigma_{\varphi\varphi})^n + (\sigma_{\varphi\varphi} - \sigma_3)^n + (\sigma_1 - \sigma_3)^n = 2\sigma_0^n. \quad (1)$$

Here  $1 \leq n < \infty$  and  $\sigma_0$  is the tensile yield stress. In the case of perfectly plastic materials, the latter is a constitutive parameter. Equation (1) assumes that

$$\sigma_1 \geq \sigma_{\varphi\varphi} \text{ and } \sigma_3 \leq \sigma_{\varphi\varphi}. \quad (2)$$

This assumption should be verified a posteriori. The elastic strains are neglected. The principal strain rate components are denoted as  $\xi_1$ ,  $\xi_{\varphi\varphi}$ , and  $\xi_3$ . In addition,  $\xi_{\varphi\varphi}$  is the circumferential strain rate. The other non-zero strain rate components in the spherical coordinate system are  $\xi_{\rho\rho}$ ,  $\xi_{\theta\theta}$ , and  $\xi_{\rho\theta}$ . The plastic flow rule associated with the yield criterion (1) is

$$\xi_1 = \lambda \left[ (\sigma_1 - \sigma_{\varphi\varphi})^{n-1} + (\sigma_1 - \sigma_3)^{n-1} \right], \xi_{\varphi\varphi} = \lambda \left[ (\sigma_{\varphi\varphi} - \sigma_3)^{n-1} - (\sigma_1 - \sigma_{\varphi\varphi})^{n-1} \right], \xi_3 = -\lambda \left[ (\sigma_{\varphi\varphi} - \sigma_3)^{n-1} + (\sigma_1 - \sigma_3)^{n-1} \right]. \quad (3)$$

Here  $\lambda$  is a non-negative multiplier.

The stress boundary conditions are

$$\sigma_{\rho\theta} = 0 \quad (4)$$

for  $\theta = 0$  and

$$\sigma_{\rho\theta} = \tau_m \quad (5)$$

for  $\theta = \theta_0$ . Here  $\tau_m$  is the shear yield stress. Condition (5) is necessary for the existence of the strain rate intensity factor [14]. It follows from (1) that

$$\tau_m = \frac{\sigma_0}{\sqrt{1 + 2^{n-1}}}. \quad (6)$$

### 3. General Solution

The method proposed in [13] for predicting the evolution of material properties near frictional interfaces in metal forming processes requires the theoretical strain rate intensity factor. The only available numerical method for calculating the strain rate intensity factor is restricted to plane strain problems [16]. In many cases, a reasonable approximate solution for extrusion and drawing through conical dies can be based on solutions for the flow of plastic material through an infinite converging channel [17]. This approach is adopted in the present paper. The general solutions required were derived in [19,20]. The solution [20] is more convenient if the yield criterion is written in terms of the principal stresses. Therefore, this solution is adapted and modified below for calculating the strain rate intensity factor.

Let  $\psi$  be the angle between the axis  $\rho$  and the direction of the principal stress  $\sigma_3$  measured from the axis clockwise (Figure 2).

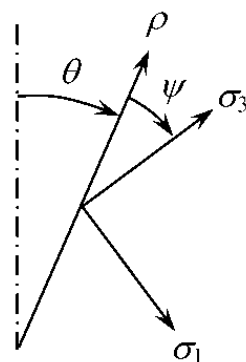


Figure 2. Orientation of the principal stresses.

The transformation equations for the components of tensors in a generic  $(\rho, \theta)$  plane lead to

$$\sigma_{\rho\rho} = \frac{1}{2}(\sigma_1 + \sigma_3) - \frac{1}{2}(\sigma_1 - \sigma_3) \cos 2\psi, \quad \sigma_{\theta\theta} = \frac{1}{2}(\sigma_1 + \sigma_3) + \frac{1}{2}(\sigma_1 - \sigma_3) \cos 2\psi, \quad \sigma_{\rho\theta} = -\frac{1}{2}(\sigma_1 - \sigma_3) \sin 2\psi \quad (7)$$

and

$$\tilde{\zeta}_{\rho\rho} = \frac{1}{2}(\tilde{\zeta}_1 + \tilde{\zeta}_3) - \frac{1}{2}(\tilde{\zeta}_1 - \tilde{\zeta}_3) \cos 2\psi, \quad \tilde{\zeta}_{\theta\theta} = \frac{1}{2}(\tilde{\zeta}_1 + \tilde{\zeta}_3) + \frac{1}{2}(\tilde{\zeta}_1 - \tilde{\zeta}_3) \cos 2\psi, \quad \tilde{\zeta}_{\rho\theta} = -\frac{1}{2}(\tilde{\zeta}_1 - \tilde{\zeta}_3) \sin 2\psi. \quad (8)$$

The direction of flow dictates that  $\sigma_{\rho\theta} \geq 0$  and  $\sigma_{\rho\rho} \geq \sigma_{\theta\theta}$ . Then, it follows from (7) that  $\sin 2\psi \leq 0$  and  $\cos 2\psi \leq 0$ . Consequently,

$$-\frac{\pi}{2} \leq \psi \leq -\frac{\pi}{4}. \quad (9)$$

Introduce the following stress variables:

$$s_1 = \sigma_1 - \sigma_{\varphi\varphi}, \quad s_2 = \sigma_{\varphi\varphi} - \sigma_3, \quad \text{and} \quad s_3 = \sigma_1 - \sigma_3. \quad (10)$$

It is seen from (2) that  $s_1 \geq 0$ ,  $s_2 \geq 0$ , and  $s_3 > 0$ . Equations (3) and (10) combine to give

$$\tilde{\zeta}_1 + \tilde{\zeta}_3 = \lambda(s_1^{n-1} - s_2^{n-1}), \quad \tilde{\zeta}_1 - \tilde{\zeta}_3 = \lambda(2s_3^{n-1} + s_2^{n-1} + s_1^{n-1}) \quad \text{and} \quad \tilde{\zeta}_{\varphi\varphi} = \lambda(s_2^{n-1} - s_1^{n-1}). \quad (11)$$

Substituting the first two equations in (11) into (8), one gets

$$\begin{aligned} \tilde{\zeta}_{\rho\rho} &= \frac{\lambda}{2} \left[ s_1^{n-1} - s_2^{n-1} - (2s_3^{n-1} + s_2^{n-1} + s_1^{n-1}) \cos 2\psi \right], \\ \tilde{\zeta}_{\theta\theta} &= \frac{\lambda}{2} \left[ s_1^{n-1} - s_2^{n-1} + (2s_3^{n-1} + s_2^{n-1} + s_1^{n-1}) \cos 2\psi \right], \\ \tilde{\zeta}_{\rho\theta} &= -\frac{\lambda}{2} (2s_3^{n-1} + s_2^{n-1} + s_1^{n-1}) \sin 2\psi. \end{aligned} \quad (12)$$

Eliminating  $\lambda$  between the third equation in (11) and the second equation in (12) yields

$$\frac{\tilde{\zeta}_{\varphi\varphi}}{\tilde{\zeta}_{\theta\theta}} = \frac{2(s_2^{n-1} - s_1^{n-1})}{s_1^{n-1} - s_2^{n-1} + (2s_3^{n-1} + s_2^{n-1} + s_1^{n-1}) \cos 2\psi}. \quad (13)$$

The other independent equations that follow from (12) are the equation of incompressibility

$$\tilde{\zeta}_{\rho\rho} + \tilde{\zeta}_{\theta\theta} + \tilde{\zeta}_{\varphi\varphi} = 0 \quad (14)$$

and

$$\frac{2\tilde{\zeta}_{\rho\theta}}{\tilde{\zeta}_{\rho\rho} - \tilde{\zeta}_{\theta\theta}} = \tan 2\psi. \quad (15)$$

The radial velocity found in [20] can be written as

$$u_r = -\frac{u}{\rho^2}. \quad (16)$$

Here  $u > 0$  is an arbitrary function of  $\theta$ . The other velocity components vanish. This velocity field satisfies (14). Moreover,  $\tilde{\zeta}_{\theta\theta} = \tilde{\zeta}_{\varphi\varphi}$  and Equation (13) becomes

$$\frac{2(s_2^{n-1} - s_1^{n-1})}{s_1^{n-1} - s_2^{n-1} + (2s_3^{n-1} + s_2^{n-1} + s_1^{n-1}) \cos 2\psi} = 1. \quad (17)$$

One can express the strain rate components involved in (15) through  $u$  using (16). As a result,

$$\xi_{\rho\theta} = \frac{3u \tan 2\psi}{2\rho^3} \text{ and } \frac{du}{d\theta} = 3u \tan 2\psi. \quad (18)$$

Substituting (10) into (1), one can find

$$s_1^n + s_2^n + s_3^n = 2\sigma_0^n. \quad (19)$$

Equations (17) and (19) should be supplemented with the identity:

$$s_1 + s_2 - s_3 = 0. \quad (20)$$

The general structure of Equation (17) through (20) suggests that all quantities involved in these equations are independent of  $\rho$ . The solution below is based on this assumption.

It remains to consider the equilibrium equations. In the case under consideration, these equations read

$$\begin{aligned} \rho \frac{\partial \sigma_{\rho\rho}}{\partial \rho} + \frac{d\sigma_{\rho\theta}}{d\theta} + (2\sigma_{\rho\rho} - \sigma_{\theta\theta} - \sigma_{\varphi\varphi} + \sigma_{\rho\theta} \cot \theta) &= 0, \\ \frac{\partial \sigma_{\theta\theta}}{\partial \theta} + (\sigma_{\theta\theta} - \sigma_{\varphi\varphi}) \cot \theta + 3\sigma_{\rho\theta} &= 0. \end{aligned} \quad (21)$$

The equations in (21) are compatible if

$$\sigma_{\rho\rho} = -A\sigma_0 \ln \rho + s_{\rho\rho}(\theta), \quad \sigma_{\theta\theta} = -A\sigma_0 \ln \rho + s_{\theta\theta}(\theta), \text{ and } \sigma_{\varphi\varphi} = -A\sigma_0 \ln \rho + s_{\varphi\varphi}(\theta). \quad (22)$$

Here  $A$  is constant, and  $s_{\rho\rho}(\theta)$ ,  $s_{\theta\theta}(\theta)$ , and  $s_{\varphi\varphi}(\theta)$  are arbitrary functions of  $\theta$ . In particular, the equations in (21) become

$$\frac{d\sigma_{\rho\theta}}{d\theta} + 2s_{\rho\rho} - s_{\theta\theta} - s_{\varphi\varphi} + \sigma_{\rho\theta} \cot \theta = A\sigma_0 \text{ and } \frac{ds_{\theta\theta}}{d\theta} + (s_{\theta\theta} - s_{\varphi\varphi}) \cot \theta + 3\sigma_{\rho\theta} = 0. \quad (23)$$

It follows from (7), (10), and (22) that

$$\begin{aligned} \sigma_{\rho\rho} - \sigma_{\theta\theta} = s_{\rho\rho} - s_{\theta\theta} = -s_3 \cos 2\psi, \quad \sigma_{\rho\rho} - \sigma_{\varphi\varphi} = s_{\rho\rho} - s_{\varphi\varphi} = \frac{s_1 - s_2}{2} - \frac{s_3 \cos 2\psi}{2}, \\ \sigma_{\theta\theta} - \sigma_{\varphi\varphi} = s_{\theta\theta} - s_{\varphi\varphi} = \frac{s_1 - s_2}{2} + \frac{s_3 \cos 2\psi}{2}, \quad \sigma_{\rho\theta} = -\frac{s_3 \sin 2\psi}{2}. \end{aligned} \quad (24)$$

Substituting (24) into (23) yields

$$\begin{aligned} 2s_3 \cos 2\psi \frac{d\psi}{d\theta} + \sin 2\psi \frac{ds_3}{d\theta} + 3s_3 \cos 2\psi - s_1 + s_2 + s_3 \sin 2\psi \cot \theta &= -2A\sigma_0, \\ \frac{ds_{\theta\theta}}{d\theta} + \frac{1}{2}(s_1 - s_2 + s_3 \cos 2\psi) \cot \theta - \frac{3}{2}s_3 \sin 2\psi &= 0. \end{aligned} \quad (25)$$

The second equation can be solved after  $s_1$ ,  $s_2$ ,  $s_3$ , and  $\psi$  are found. Its solution is not required for calculating the strain rate intensity factor. Therefore, this equation will not be considered below. Moreover, the only difference between extrusion and drawing appears in the boundary condition to this equation. Therefore, the derivation below is valid for both processes.

The first equation in (25) should be solved numerically together with Equations (17), (19) and (20). Taking into account (7) and (9), one can rewrite the boundary conditions (4) and (5) as

$$\psi = -\frac{\pi}{2} \quad (26)$$

for  $\theta = 0$  and

$$\psi = -\frac{\pi}{4} \quad (27)$$

for  $\theta = \theta_0$ . The solution of the first equation in (25) satisfying these boundary conditions determines  $A$ .

#### 4. Strain Rate and Work Rate Intensity Factors

The strain rate intensity factor was introduced in [14]. This factor is the coefficient of the leading singular term in the expansion of the quadratic invariant of the strain rate tensor in a series in the vicinity of maximum friction surfaces. One can introduce other definitions resulting from the same singular behavior of the velocity field. All these definitions are equivalent from the mathematical point of view. In particular, it is straightforward to calculate the strain rate intensity factor according to any definition if it is known according to one of these definitions. However, it is important to choose a physically reasonable definition for using the strain rate intensity factor in constitutive equations. One of the best candidates is the work rate intensity factor [21]. This factor is adopted in the present paper. Its definition is given by

$$w = \frac{W}{\sqrt{z}} + o\left(\frac{1}{\sqrt{z}}\right) \quad (28)$$

as  $z \rightarrow 0$ . Here  $z$  is the normal distance to the friction surface,  $w$  is the plastic work rate, and  $W$  is the work rate intensity factor.

In the case under consideration, the plastic work rate is given by

$$w = \sigma_{\rho\rho}\tilde{\zeta}_{\rho\rho} + \sigma_{\theta\theta}\tilde{\zeta}_{\theta\theta} + \sigma_{\varphi\varphi}\tilde{\zeta}_{\varphi\varphi} + 2\sigma_{\rho\theta}\tilde{\zeta}_{\rho\theta}. \quad (29)$$

However, only the last term approaches infinity near the maximum friction surface. Therefore, taking into account (5) and (18), one can represent (29) as

$$w = \frac{3\tau_m u_f}{\rho^3} \tan 2\psi \quad (30)$$

to leading order. Here  $u_f$  is the value of  $u$  at the friction surface. Using (27), one transforms (30) to

$$w = -\frac{3\tau_m u_f}{2\rho^3} \left(\psi + \frac{\pi}{4}\right)^{-1} + o\left[\left(\psi + \frac{\pi}{4}\right)^{-1}\right] \quad (31)$$

as  $\psi \rightarrow -\pi/4$ . Comparing (28) and (31) shows that

$$\psi + \frac{\pi}{4} = -K\sqrt{\theta_0 - \theta} + o\left(\sqrt{\theta_0 - \theta}\right) \quad (32)$$

as  $\theta \rightarrow \theta_0$ . Here  $K > 0$  is constant. Moreover,

$$W = \frac{3\tau_m u_f}{2K\rho^{5/2}}. \quad (33)$$

One should conduct an asymptotic analysis near the friction surface to find  $K$ . The boundary condition (5) demands  $s_1 = \tau_m$ ,  $s_2 = \tau_m$ , and  $s_3 = 2\tau_m$  at  $\theta = \theta_0$  (or  $\psi = -\pi/4$ ). These quantities can be regarded as functions of  $\psi$ . Then,

$$\begin{aligned} \frac{s_1}{\tau_m} &= 1 + \alpha_1^{(0)}\left(\psi + \frac{\pi}{4}\right) + \alpha_1^{(1)}\left(\psi + \frac{\pi}{4}\right)^2 + o\left[\left(\psi + \frac{\pi}{4}\right)^2\right], \\ \frac{s_2}{\tau_m} &= 1 + \alpha_2^{(0)}\left(\psi + \frac{\pi}{4}\right) + \alpha_2^{(1)}\left(\psi + \frac{\pi}{4}\right)^2 + o\left[\left(\psi + \frac{\pi}{4}\right)^2\right], \\ \frac{s_3}{\tau_m} &= 2 + \alpha_3^{(0)}\left(\psi + \frac{\pi}{4}\right) + \alpha_3^{(1)}\left(\psi + \frac{\pi}{4}\right)^2 + o\left[\left(\psi + \frac{\pi}{4}\right)^2\right] \end{aligned} \quad (34)$$

as  $\psi \rightarrow -\pi/4$ . Moreover,

$$\cos 2\psi = 2\left(\psi + \frac{\pi}{4}\right) + O\left[\left(\psi + \frac{\pi}{4}\right)^3\right] \quad (35)$$

as  $\psi \rightarrow -\pi/4$ . Substituting (34) and (35) into (17), (19), and (20), one gets

$$\begin{aligned} \alpha_1^{(0)} = -\alpha_2^{(0)} = \alpha_0, \alpha_3^{(0)} = 0, \alpha_1^{(1)} = \alpha_2^{(1)} = \alpha_1, \alpha_3^{(1)} = 2\alpha_1, \\ \alpha_0 = \frac{2+2^n}{3(1-n)}, \alpha_1 = \frac{2+2^n}{9(1-n)}. \end{aligned} \quad (36)$$

The first equation in (25) can be transformed to

$$\left(2s_3 \cos 2\psi + \sin 2\psi \frac{ds_3}{d\psi}\right) \frac{d\psi}{d\theta} + 3s_3 \cos 2\psi - s_1 + s_2 + s_3 \sin 2\psi \cot \theta = -2A\sigma_0 \quad (37)$$

The derivative  $ds_3/d\psi$  is readily determined from (34). Then, upon substitution from (34)–(36), Equation (37) supplies

$$\frac{d\psi}{d\theta} = \frac{9(n-1)\left(\cot \theta_0 - A\sqrt[n]{1+2^{n-1}}\right)}{4[9(n-1)+1+2^{n-1}]} \left(\psi + \frac{\pi}{4}\right)^{-1} + o\left[\left(\psi + \frac{\pi}{4}\right)^{-1}\right] \quad (38)$$

as  $\psi \rightarrow -\pi/4$ . Differentiating (32) yields

$$\frac{d\psi}{d\theta} = -\frac{K^2}{2} \left(\psi + \frac{\pi}{4}\right)^{-1} + o\left[\left(\psi + \frac{\pi}{4}\right)^{-1}\right] \quad (39)$$

as  $\psi \rightarrow -\pi/4$ . Comparing (38) and (39) shows that

$$K = \frac{3}{\sqrt{2}} \sqrt{\frac{(n-1)\left(A\sqrt[n]{1+2^{n-1}} - \cot \theta_0\right)}{9(n-1)+1+2^{n-1}}}. \quad (40)$$

Then, the work rate intensity factor is found from (6), (33) and (40) as

$$W = \frac{\sigma_0 u_f}{\sqrt{2} \sqrt[n]{1+2^{n-1}} \sqrt{n-1} \rho^{5/2}} \sqrt{\frac{9(n-1)+1+2^{n-1}}{A\sqrt[n]{1+2^{n-1}} - \cot \theta_0}}. \quad (41)$$

The solution of the second equation in (18) can be represented as

$$u = u_f \exp\left(3 \int_{\theta_0}^{\theta} \tan 2\psi d\theta\right). \quad (42)$$

It is understood here that the solution of Equation (37) provides  $\psi$  as a function of  $\theta$ . A subsequence of the incompressibility equation is

$$\pi V_0 R_0^2 = -2\pi \int_0^{\theta_0} u_r \rho^2 \sin \theta d\theta. \quad (43)$$

Equations (16), (42) and (43) combine to give

$$\frac{V_0 R_0^2}{2} = u_f D, \quad D = \int_0^{\theta_0} \exp\left(3 \int_{\theta_0}^{\theta} \tan 2\psi d\theta\right) \sin \theta d\theta. \quad (44)$$

Then, Equation (41) becomes

$$W = \frac{\sigma_0 V_0 R_0^2}{2\sqrt{2}D \sqrt[1+2^{n-1}]{\sqrt{n-1}}} \sqrt{\frac{9(n-1)+1+2^{n-1}}{A \sqrt[1+2^{n-1}]{-\cot\theta_0}}} \rho^{-5/2}. \quad (45)$$

### 5. Thickness of the Layer of Intensive Plastic Deformation and Hardness at the Friction Surface

The empirical equations proposed in [13] involve the strain rate intensity integrated over the distance traveled by a material particle along the friction surface. The work rate intensity factor should be integrated similarly. It is seen from Figure 1 that the distance required is  $s = \rho_a - \rho$ . Here  $\rho_a$  is the  $\rho$ -coordinate of point  $a$ . The  $\rho$ -coordinate of point  $b$  is denoted as  $\rho_b$ . Then, the integrated work rate intensity factor is

$$\omega = \int_0^s W d\gamma. \quad (46)$$

Substituting (45) into (46) and replacing  $\rho$  with  $s$ , one gets

$$\begin{aligned} \omega &= \frac{\sigma_0 V_0 R_0^2}{2\sqrt{2}D \sqrt[1+2^{n-1}]{\sqrt{n-1}}} \sqrt{\frac{9(n-1)+1+2^{n-1}}{A \sqrt[1+2^{n-1}]{-\cot\theta_0}}} \int_0^s (\rho_a - \gamma)^{-5/2} d\gamma = \\ &= \frac{\sigma_0 V_0 R_0^2}{3\sqrt{2}D \sqrt[1+2^{n-1}]{\sqrt{n-1}}} \sqrt{\frac{9(n-1)+1+2^{n-1}}{A \sqrt[1+2^{n-1}]{-\cot\theta_0}}} \left[ \frac{1}{(\rho_a - s)^{3/2}} - \frac{1}{\rho_a^{3/2}} \right]. \end{aligned} \quad (47)$$

It follows from the geometry of Figure 1 that  $\rho_a = R_0/\sin\theta_0$  and  $\rho_b = r_0/\sin\theta_0$ . Then, Equation (47) becomes

$$\omega = \sigma_0 V_0 \sqrt{R_0} \omega_0 \left[ \frac{1}{(1 - s/\rho_a)^{3/2}} - 1 \right] \quad (48)$$

where  $0 \leq s/\rho_a \leq (\rho_a - \rho_b)/\rho_a = 1 - r_0/R_0$  and

$$\omega_0 = \frac{\sin^{3/2}\theta_0}{3\sqrt{2}D \sqrt[1+2^{n-1}]{\sqrt{n-1}}} \sqrt{\frac{9(n-1)+1+2^{n-1}}{A \sqrt[1+2^{n-1}]{-\cot\theta_0}}}. \quad (49)$$

Using (48), one can represent the empirical equations provided in [13] as

$$\begin{aligned} \delta &= a_1 - a_2 \exp \left\{ -a_3 V_0 \sqrt{R_0} \omega_0 \left[ \frac{1}{(1-s/\rho_a)^{3/2}} - 1 \right] \right\}, \\ H_s &= b_1 - b_2 \exp \left\{ -b_3 V_0 \sqrt{R_0} \omega_0 \left[ \frac{1}{(1-s/\rho_a)^{3/2}} - 1 \right] \right\}. \end{aligned} \quad (50)$$

Here  $\delta$  is the thickness of the layer of intensive plastic deformation generated near the friction surface. Its dimension is the micron. Consequently,  $a_1$  and  $a_2$  have the same dimension. The parameter  $a_3 V_0 \sqrt{R_0}$  is dimensionless. Additionally,  $H_s$  is the hardness at the friction surface. Its dimension is GPa. Consequently,  $b_1$  and  $b_2$  have the same dimension. The parameter  $b_3 V_0 \sqrt{R_0}$  is dimensionless. It has been found in [13] that  $a_1 = 68.3 \mu\text{m}$ ,  $a_2 = 68.6 \mu\text{m}$ ,  $a_3 = 14.6 \text{ s} \cdot \text{mm}^{-3/2}$ ,  $b_1 = 3.2 \text{ GPa}$ ,  $b_2 = 1.6 \text{ GPa}$  and  $b_3 = 10.3 \text{ s} \cdot \text{mm}^{-3/2}$  for aluminum 6061. These values of the parameters are used in the following section.

### 6. Numerical Examples

This section illustrates the solution above with numerical examples. Given Equation (50), the problem is classified by five parameters ( $V_0$ ,  $R_0$ ,  $R_0/r_0$ ,  $\theta_0$ , and  $n$ ). Therefore, no comprehensive parametric analysis is feasible. The numerical examples below focus on the

effect of  $n$  and  $\theta_0$  on the thickness of the layer of intensive plastic deformation, assuming that  $V_0 = 1 \text{ mm} \cdot \text{s}^{-1}$ ,  $R_0 = 5 \text{ mm}$ , and  $R_0/r_0 = 1.5$ . The first equation in (50) is used. The effect of  $n$  and  $\theta_0$  on the hardness at the friction surface can be investigated similarly using the second equation in (50). Figure 3 depicts the dependence of  $A$  on  $\theta_0$  at  $n = 2$  and  $n = 20$ . It is seen that the effect of the  $n$ -value is rather weak. In particular, the curves for this value in the range  $2 < n < 20$  lie between the two curves shown in the figure.

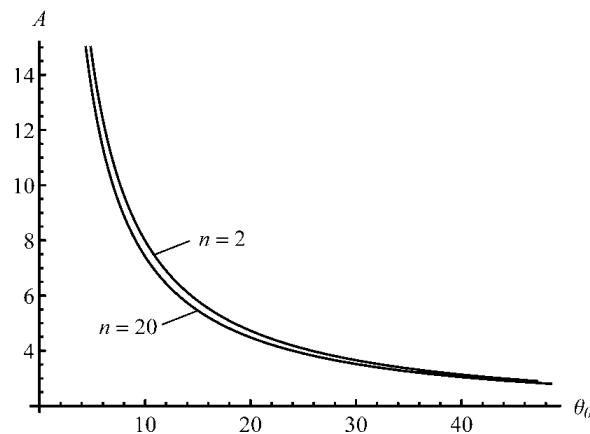


**Figure 3.** Variation of  $A$  with the die angle in the range  $2 \leq n \leq 20$ .

The thickness of the layer of intensive plastic deformation along the friction surface is shown in Figures 4–9. In particular, the curves in Figures 4 and 5 correspond to the von Mises yield criterion, assuming that  $\theta_0 = 5^\circ$  and  $\theta_0 = 45^\circ$ . Figure 4 demonstrates the increases in the thickness along the entire friction surface. It is seen that the gradient is very high after the material enters the die until the thickness becomes saturated. The saturation value is practically independent of the angle. Its effect is revealed in a region near the entrance to the die (Figure 5). Figures 6 and 7 show the thickness of the layer of intensive plastic deformation along the friction surface for several  $n$ -values, assuming that  $\theta_0 = 30^\circ$ . Figures 8 and 9 depict the same distribution for  $\theta_0 = 15^\circ$ . It is worth noting that the Taylor polycrystal model [22] predicts that  $n$  is close to 6 and 8 for BCC and FCC materials, respectively [20]. The general tendency is the same as in Figures 4 and 5. In particular, the gradient in the thickness is very high after the material enters the die until it becomes saturated (Figures 6 and 8). The effect of  $n$  is revealed in a region near the entrance to the die (Figures 7 and 9).

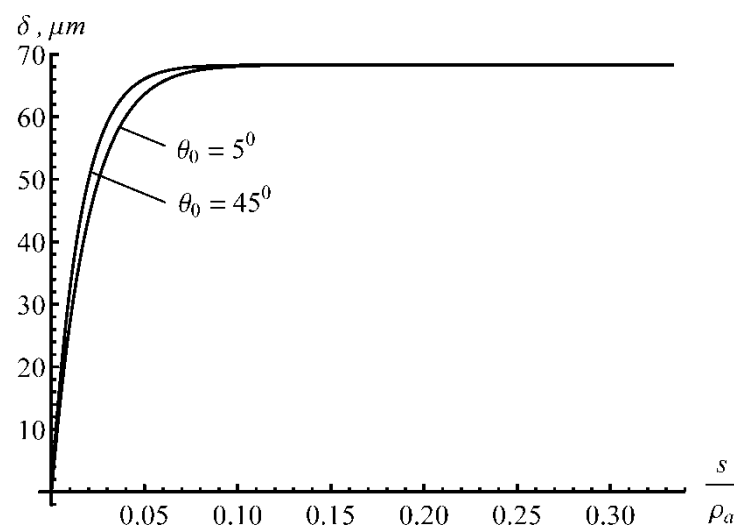


**Figure 4.** Thickness of the layer of intensive plastic deformation along the friction surface for the von Mises yield criterion.

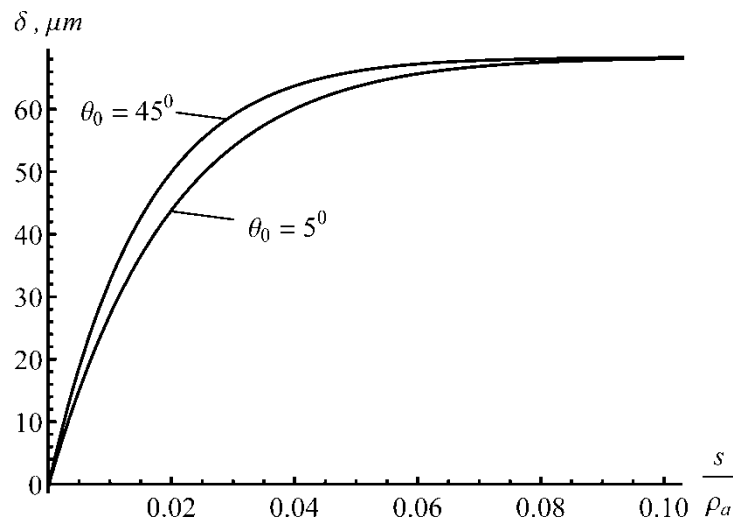


**Figure 5.** Thickness of the layer of intensive plastic deformation near the entrance to the die for the von Mises yield criterion.

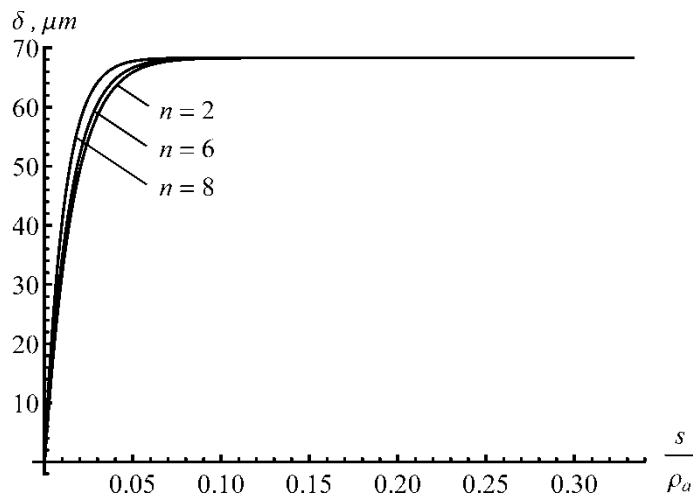


**Figure 6.** Thickness of the layer of intensive plastic deformation along the friction surface at  $\theta_0 = 30^\circ$  and different  $n$ - values.

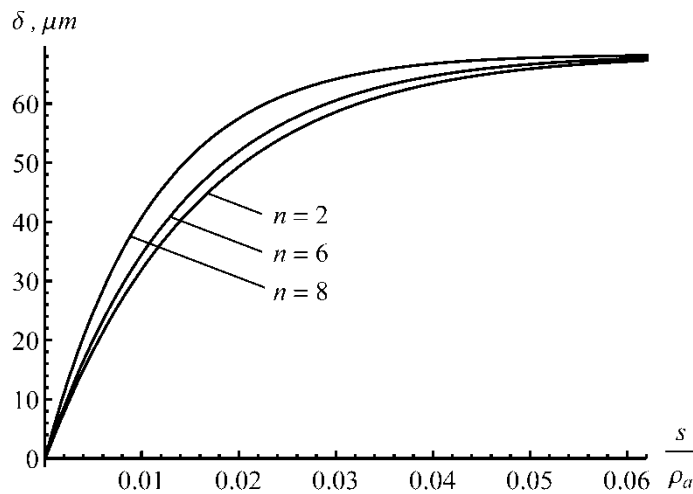


**Figure 7.** Thickness of the layer of intensive plastic deformation near the entrance to the  $\theta_0 = 30^\circ$  die and different  $n$ - values.

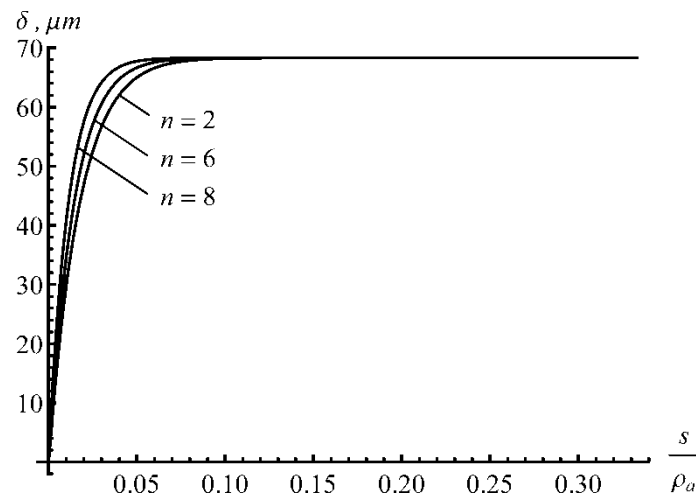


**Figure 8.** Thickness of the layer of intensive plastic deformation along the friction surface at  $\theta_0 = 15^\circ$  and different  $n$ - values.

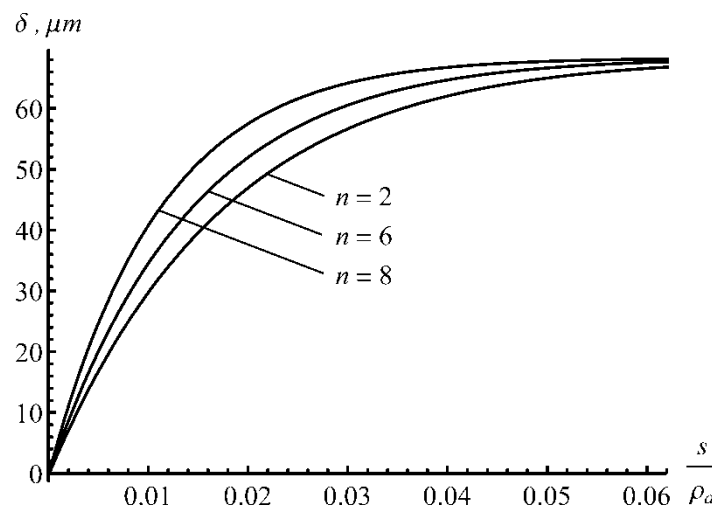


**Figure 9.** Thickness of the layer of intensive plastic deformation near the entrance to the  $\theta_0 = 15^\circ$  die and different  $n$ - values.

## 7. Discussion

The present paper provides a theoretical prediction of the thickness of the layer of intensive plastic deformation generated near the friction surface and the hardness at the friction surface in axisymmetric extrusion and drawing using the empirical equation proposed in [13]. The general solution is valid for any value of the exponent involved in Hosford's yield criterion [18]. The numerical results were presented for the thickness of the layer of intensive plastic deformation, assuming that  $n = 2$  (von Mises yield criterion),  $n = 6$  (good approximation for BCC materials), and  $n = 8$  (good approximation for FCC materials). The general tendency is that the thickness of the layer of intensive plastic deformation rapidly increases to an almost saturation value after the material near the friction surface enters the extrusion/drawing die (Figures 4, 6 and 8). The effects of  $n$ -value and the die angle are revealed in a region near the entrance to the die (Figures 5, 7 and 9). This general tendency is in agreement with physical expectations. In particular, the mode of deformation near surfaces with high friction is similar to that in traditional severe deformation processes [23]. Material properties in the latter become saturated to constant values during the initial stage of the process [24–27]. This tendency in the evolution of material properties suggests that the thickness of the layer of intensive plastic deformation

reaches an almost saturation value shortly after the material near the friction surface enters the extrusion/drawing die.

The predictive effect of the solution is that the exponent  $n$  involved in Hosford's yield criterion influences the thickness of the layer of intensive plastic deformation near frictional interfaces. It can be seen from Figure 4 through Figure 9 that this effect is comparable with the effect of the die angle. However, available experimental studies mainly focus on the latter [9–13]. The result of the present paper can be considered as an encouragement to experimentalists to attempt to verify the theoretical predictions made.

The present theoretical solution is valid for axisymmetric extrusion through a conical die. High gradients of material properties appear in other extrusion processes [28,29]. The application of the general method to such processes requires the development of a numerical method that is capable of solving singular boundary value problems.

It is straightforward to obtain numerical results for the hardness distribution along the friction surface using the general solution found and the second equation in (50).

**Funding:** This research was made possible by grant 20-79-10340 from the Russian Science Foundation.

**Institutional Review Board Statement:** Not applicable.

**Informed Consent Statement:** Not applicable.

**Data Availability Statement:** Not applicable.

**Conflicts of Interest:** The author declares no conflict of interest.

## Nomenclature

$n$	constitutive parameter involved in Hosford's yield criterion
$r_0$	final radius of the rod
$s_1, s_2, s_3$	stress variables introduced in Equation (10)
$u_r$	radial velocity
$w$	plastic work rate
$H_s$	hardness at the friction surface
$R_0$	initial radius of the rod
$W$	work rate intensity factor
$\delta$	thickness of the layer of intensive plastic deformation
$\theta_0$	die semi-angle
$\zeta_{\rho\rho}, \zeta_{\varphi\varphi}, \zeta_{\theta\theta}, \zeta_{\rho\theta}$	strain rate components referred to the spherical coordinate system
$\xi_1, \xi_3$	principal strain rates
$(\rho, \theta, \varphi)$	spherical coordinate system
$\sigma_{\rho\rho}, \sigma_{\varphi\varphi}, \sigma_{\theta\theta}, \sigma_{\rho\theta}$	stress components referred to the spherical coordinate system
$\sigma_0$	tensile yield stress
$\sigma_1, \sigma_3$	principal stresses
$\tau_m$	shear yield stress
$\psi$	angle between the axis $\rho$ and the direction of the principal stress $\sigma_3$
$\omega$	integrated work rate intensity factor

## References

1. Griffiths, B.J. Mechanisms of white layer generation with reference to machining and deformation processes. *ASME J. Tribol.* **1987**, *109*, 525–530. [[CrossRef](#)]
2. Griffiths, B.J.; Furze, D.C. Tribological advantages of white layers produced by machining. *ASME J. Tribol.* **1987**, *109*, 338–342. [[CrossRef](#)]
3. Choi, Y. Influence of a white layer on the performance of hard machined surfaces in rolling contact. *Proc. Inst. Mech. Eng. B J. Eng. Manuf.* **2010**, *224*, 1207–1215. [[CrossRef](#)]
4. Murai, T.; Matsuoka, S.; Miyamoto, S.; Oki, Y. Effects of extrusion conditions on microstructure and mechanical properties of AZ31B magnesium alloy extrusions. *J. Mater. Process. Technol.* **2003**, *141*, 207–212. [[CrossRef](#)]
5. Kajino, S.; Asakawa, M. Effect of "additional shear strain layer" on tensile strength and microstructure of fine drawn wire. *J. Mater. Process. Technol.* **2006**, *177*, 704–708. [[CrossRef](#)]

6. Uematsu, Y.; Tokaji, K.; Kamakura, M.; Uchida, K.; Shibata, H.; Bekku, N. Effect of extrusion conditions on grain refinement and fatigue behaviour in magnesium alloys. *J. Mater. Sci. Eng. A* **2006**, *434*, 131–140. [[CrossRef](#)]
7. Tang, W.; Huang, S.; Zhang, S.; Li, D.; Peng, Y. Influence of extrusion parameters on grain size and texture distributions of AZ31 alloy. *J. Mater. Process. Technol.* **2011**, *211*, 1203–1209. [[CrossRef](#)]
8. Sanabria, V.; Mueller, S.; Reimers, W. Microstructure evolution of friction boundary layer during extrusion of AA 6060. *Procedia Eng.* **2014**, *81*, 586–591. [[CrossRef](#)]
9. Alexandrov, S.; Jeng, Y.-R.; Hwang, Y.-M. Generation of a fine grain layer in the vicinity of frictional interfaces in direct extrusion of AZ31 alloy. *ASME J. Manuf. Sci. Eng.* **2015**, *137*, 051003. [[CrossRef](#)]
10. Hwang, Y.-M.; Huang, T.-H.; Alexandrov, S. Manufacture of gradient microstructures of magnesium alloys using two—Stage extrusion dies. *Steel Res. Int.* **2015**, *86*, 956–961. [[CrossRef](#)]
11. Stolyarov, A.; Polyakova, M.; Atangulova, G.; Alexandrov, S.; Lang, L. Effect of frictional conditions on the generation of fine grain layers in drawing of thin steel wires. *Metals* **2019**, *9*, 819. [[CrossRef](#)]
12. Stolyarov, A.; Polyakova, M.; Atangulova, G.; Alexandrov, S. Effect of die angle and frictional conditions on fine grain layer generation in multi-pass drawing of high carbon steel wire. *Metals* **2020**, *10*, 1462. [[CrossRef](#)]
13. Alexandrov, S.; Jeng, Y.-R.; Kuo, C.-Y.; Chen, C.-Y. Towards the theoretical/experimental description of the evolution of material properties near frictional interfaces in metal forming processes. *Trib. Int.* **2022**, *171*, 107518. [[CrossRef](#)]
14. Alexandrov, S.; Richmond, O. Singular plastic flow fields near surfaces of maximum friction stress. *Int. J. Non-Linear Mech.* **2001**, *36*, 1–11. [[CrossRef](#)]
15. Facchinetti, M.; Miszuris, W. Analysis of the maximum friction condition for green body forming in an ANSYS environment. *J. Eur. Ceram. Soc.* **2016**, *36*, 2295–2302. [[CrossRef](#)]
16. Alexandrov, S.; Kuo, C.-Y.; Jeng, Y.-R. A numerical method for determining the strain rate intensity factor under plane strain conditions. *Cont. Mech. Therm.* **2016**, *28*, 977–992. [[CrossRef](#)]
17. Durban, D. Radial flow simulation of drawing and extrusion of rigid/hardening materials. *Int. J. Mech. Sci.* **1983**, *25*, 27–39. [[CrossRef](#)]
18. Hosford, W.F. A generalized isotropic yield criterion. *Trans. ASME J. Appl. Mech.* **1972**, *39*, 607–609. [[CrossRef](#)]
19. Shield, R.T. Plastic flow in a converging conical channel. *J. Mech. Phys. Solids.* **1955**, *3*, 246–258. [[CrossRef](#)]
20. Alexandrov, S.; Barlat, F. Modeling axisymmetric flow through a converging channel with arbitrary yield condition. *Acta Mech.* **1999**, *133*, 57–68. [[CrossRef](#)]
21. Alexandrov, S.; Mustafa, Y. The strain rate intensity factor in the plane strain compression of thin anisotropic metal strip. *Meccanica* **2014**, *49*, 2901–2906. [[CrossRef](#)]
22. Taylor, G.I. Plastic strains in metals. *J. Inst. Metals* **1938**, *62*, 307–324.
23. Alexandrov, S.E.; Goldstein, R.V. The similarity of grain-size evolution near frictional interfaces and in the process of equal-channel angular pressing. *Dokl. Phys.* **2013**, *58*, 177–180. [[CrossRef](#)]
24. Wetscher, F.; Vorhauer, A.; Stock, R.; Pippan, R. Structural refinement of low alloyed steels during severe plastic deformation. *Mater. Sci. Eng.* **2004**, *387–389*, 809–816. [[CrossRef](#)]
25. Pippan, R.; Wetscher, F.; Hafok, M.; Vorhauer, A.; Sabirov, I. The limits of refinement by severe plastic deformation. *Adv. Eng. Mater.* **2006**, *8*, 1046–1056. [[CrossRef](#)]
26. Xun, Y.; Mohamed, F.A. Refining efficiency and capability of top-down synthesis of nanocrystalline materials. *Mater. Sci. Eng.* **2011**, *528*, 5446–5452. [[CrossRef](#)]
27. Mohamed, F.A.; Dheda, S.S. On the minimum grain size obtainable by equal channel angular pressing. *Mater. Sci. Eng.* **2013**, *580*, 227–230. [[CrossRef](#)]
28. Zhou, W.; Yu, J.; Lin, J.; Dean, T.A. Effects of die land length and geometry on curvature and effective strain of profiles produced by a novel sideways extrusion process. *J. Mater. Process. Technol.* **2020**, *282*, 116682. [[CrossRef](#)]
29. Zhou, W.; Yu, J.; Lu, X.; Lin, J.; Dean, T.A. A comparative study on deformation mechanisms, microstructures and mechanical properties of wide thin-ribbed sections formed by sideways and forward extrusion. *Int. J. Mach. Tools Manuf.* **2021**, *168*, 103771. [[CrossRef](#)]